JACS
JOURNAL OF THE AMERICAN CHEMICAL SOCIETY

Communication

pubs.acs.org/JACS

Self-Assembly of Inorganic Nanoparticle Vesicles and Tubules Driven by Tethered Linear Block Copolymers

Jie He, Yijing Liu, Taarika Babu, Zengjiang Wei, and Zhihong Nie*

Department of Chemistry and Biochemistry, University of Maryland, College Park, Maryland 20742, United States

Supporting Information

ABSTRACT: Controllable self-assembly of nanoscale building blocks into larger specific structures provides an effective route for the fabrication of new materials with unique optical, electronic, and magnetic properties. The ability of nanoparticles (NPs) to self-assemble like molecules is opening new research frontiers in nanoscience and nanotechnology. We present a new class of amphiphilic "colloidal molecules" (ACMs) composed of inorganic NPs tethered with amphiphilic linear block copolymers (BCPs). Driven by the conformational changes of tethered BCP chains, such ACMs can self-assemble into well-defined vesicular and tubular nanostructures comprising a monolayer shell of hexagonally packed NPs in selective solvents. The morphologies and geometries of these assemblies can be controlled by the size of NPs and molecular weight of BCPs. Our approach also allows us to control the interparticle distance, thus fine-tuning the plasmonic properties of the assemblies of metal NPs. This strategy provides a general means to design new building blocks for assembling novel functional materials and devices.

Organization of nanoparticles (NPs) into 1D, 2D, or 3D hierarchical architectures could lead to a new generation of functional materials and devices.[1] As a result of, e.g., plasmonic coupling and plasmon−exciton and magnetic−magnetic interactions between these NPs, collective properties that differ from those of their individual or bulk materials emerge from the spatially ordered assembly of NPs. Over the past decade, great progress has been achieved in controlled assembly of metal NPs into various ordered or discrete nanostructures using templating (e.g., carbon nanotubes),[2] external fields (e.g., electric and magnetic fields),[3] biomolecular recognition (e.g., DNAs),[4] and directional physical or chemical binding.[5] Inspired by well-established molecular self-assembly, e.g., lipids, surfactants, and block copolymers (BCPs), the concept of amphiphilic "colloidal molecules" (ACMs) was recently proposed and explored to achieve controlled assembly of NPs.[1b,6] ACMs are generally created by decorating the surface of NPs with hydrophilic/hydrophobic polymers or small molecules.[7] Driven by the directional interactions induced by molecular tethers, the ACMs can thus spontaneously organize into the desired entities.[6a,b,7b,8] Despite tremendous development in recent years, it still remains a great challenge to develop a general methodology to create ACMs with well-defined surface chemistry that enables their organization into desired hierarchical nanoarchitectures for targeted applications.

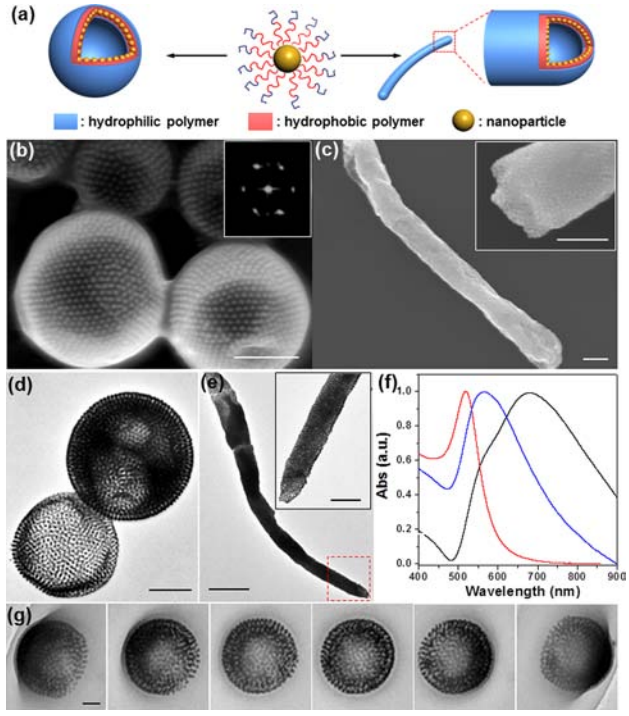

Figure 1. (a) Amphiphilic BCP-assisted self-assembly of NPs into vesicles or tubules. (b−e) Representative SEM (b,c) and TEM (d,e) images of vesicles (b,d) and tubules (c,e) obtained from self-assembly of Au-P1 and Au-P2, respectively. Inset in (b) is the FFT pattern of SEM images. (f) UV−vis spectra of individual AuNPs, vesicles, and tubules (from left to right), indicating tunable plasmonic coupling of AuNP assemblies. (g) TEM images of vesicles at different tilting angles (left to right: −60°, −40°, −20°, 0°, 30°, and 60°). Scale bars: 200 nm in (b−d) and insets of (c,e), 500 nm in (e), and 100 nm in (g).

Here we report the rational design of a new type of ACMs, grafting linear amphiphilic BCPs onto the surface of NPs and their self-assembly into various nanostructures, e.g., vesicles and tubules in selective solvents (Figure 1a). Self-assembly of ACMs is driven by the colloidal amphiphilicity originated by the conformational rearrangement of grafted BCPs. Compared to NPs tethered by mixed homopolymer brushes,[7,8a] in which the different bonding strengths and absorption kinetics of different polymers onto NPs make it difficult to quantitatively

Received: April 3, 2012
Published: July 2, 2012

   dx.doi.org/10.1021/ja3032295 | J. Am. Chem. Soc. 2012, 134, 11342−11345

control or predict the relative density of each type of polymer, BCP tethers offer greater control over the chemical functionality and composition (i.e., relative volume of hydrophilic/hydrophobic moieties) as well as architectural complexity of polymer chains on NP surface. Mobility of the junction points of BCP chains enables reconfiguration of the interface of the constituent blocks of BCPs on the NP surface, leading to new assembly behaviors of colloidal building blocks. Self-assembly of our ACMs is largely determined by the relative sizes of NPs and BCPs, analogous to but different from the amphiphilic small molecules or BCPs.[9] When BCPs with a long hydrophobic block or NPs with large diameters were used, the ACMs self-assembled into vesicles, while tubular assemblies were generated for ACMs comprising BCPs with a shorter hydrophobic block and NPs with smaller sizes. To the best of our knowledge, this is the first report of polymer-assisted NP assembly into tubular nanostructures. The interparticle distance between AuNPs in the assemblies can be tuned to achieve control over the plasmonic properties of assembled structures by varying the molecular length of hydrophobic blocks. This general approach can be extended to assemble NPs with different dimensions and geometries (i.e., nanorods and nanocubes).

As a prototype system, we used 14 nm AuNPs carrying amphiphilic BCPs of poly(2-(2-methoxyethoxy)ethyl methacrylate)-*block*-polystyrene ($PMEO_2MA$-*b*-PS) or poly(ethyl oxide)-*block*-polystyrene (PEO-*b*-PS) (Table 1). Amphiphilic BCPs of P1−P7 with PS end terminated with a thiol group were synthesized using reversible addition−fragmentation chain-transfer (RAFT) polymerization, followed by the reduction of dithioester to thiol in the presence of butyl amine (see Supporting Information (SI) for synthetic details). The amphiphilic BCPs are grafted onto the surface of AuNPs via covalent Au−S bonds using the solution ligand exchange approach.[6b] The polymer-modified AuNPs were centrifuged for at least 6−8 cycles to remove free polymers, and the concentration of residual free polymers present in the final solution is estimated to be below 10^{-16} M. AuNPs functionalized with BCPs are hereafter denoted as Au-P*N* in which *N* represents the sample number, as listed in Table 1. The average grafting density of BCPs is estimated to be ∼0.10 nm^{-2} by measuring the thickness of the polymer shell on AuNPs in high magnification SEM images (see calculation in SI). This value corresponds to ∼63 chains per 14-nm AuNP. We verified that for most studied Au-BCPs, the polymer chains on the surface of NPs are in a brush state in good solvents as indicated by $\langle R_0 \rangle / l > 3$, where $\langle R_0 \rangle$ and l are the average root-mean-square end-to-end distance and the average distance between grafting points of BCPs, respectively (Table S1).[10] The BCP-tethered AuNPs are well-dispersed in good solvents for both constituent blocks, e.g., THF, DMF, and chloroform. In addition, these AuNPs exhibited the amphiphilic feature, as they preferably stayed at the water/chloroform interface to minimize interfacial energy. It implies that, instead of behaving as static sandwich layers, BCPs on the AuNP surfaces can thermodynamically self-adapt to the changes in the environment by adjusting their chain conformations.

Assembly of such BCP-tethered AuNPs was triggered by the film rehydration method widely used for preparation of lipid or copolymer vesicles. Briefly, a solution of BCP-modified AuNPs in THF was first dried to form a thin film on a glass substrate under N_2 stream, followed by rehydration in water (a poor solvent for PS) with sonication or heating. Other approaches

Table 1. Synthesis and Characterization of Amphiphilic BCPs

		M_n (kg/mol)			
sample	compositions	GPC[a]	NMR[b]	PDI	R_0
P1	$PMEO_2MA_{66}$-*b*-PS_{376}-SH	40.2	51.5	1.24	13.1
P2	PEO_{45}-*b*-PS_{55}-SH	6.2	7.7	1.18	5.0
P3	PEO_{45}-*b*-PS_{114}-SH	9.7	13.9	1.11	7.2
P4	PEO_{45}-*b*-PS_{211}-SH	16.0	23.9	1.15	9.8
P5	PEO_{45}-*b*-PS_{245}-SH	18.1	25.7	1.12	10.5
P6	PEO_{45}-*b*-PS_{304}-SH	24.0	33.6	1.20	11.7
P7	PEO_{45}-*b*-PS_{455}-SH	30.2	49.3	1.18	14.2

[a]Number-average molecular weight determined by GPC using polystyrene standards for calibration. [b]Molecular weight calculated from ^{1}H NMR measurements. [c]Mean square end-to-end distance of PS blocks, calculated from $R_0 = bN^{0.5}$, where b is the Kuhn length (b = 0.18 nm for PS) and N is the number of Kuhn segments.[10]

can be also used to trigger the self-assembly of NPs. For example, we observed the formation of vesicular structures when mixing Au nanorods in THF with water. SEM and TEM images in Figure 1b−e present the well-defined vesicles and 1D tubules assembled from 14 nm AuNPs tethered with P1 and P2, respectively (see Figures S4−S7 for more images). The vesicles and tubules are composed of a monolayer shell of hexagonally packed AuNPs with defects, as confirmed by the corresponding fast Fourier transform (FFT) pattern of high-magnification SEM images. The average size of vesicles is ∼270 nm, while the average diameter of the tubules was ∼360 nm, with length up to several micrometers. The tubules showed a tendency to branch out (see Figure S7). Formation of assemblies in aqueous solutions was confirmed by dynamic light scattering (DLS). For example, before and after the formation of vesicles, the hydrodynamic diameter (D_h) of AuNPs and assemblies from DLS was 16.8 and 241.3 nm, respectively (see Figure S8), consistent with the SEM and TEM measurements. Assembly of AuNPs significantly reduced the interparticle distance (D_{Au}), leading to a red-shift in extinction spectra due to enhanced plasmonic coupling between adjacent AuNPs. Upon the formation of vesicles, the surface plasmon resonance (SPR) peaks shifted from 518 to 560 nm (Figure 1c). For the tubular assemblies, the presence of two plasmonic bands (shoulder at 678 and 560 nm) suggests the formation of 1D linear aggregates whose SPR is split into two modes: a maximum and a weak absorption peak corresponding to the longitudinal and transverse plasmonic modes, respectively. This resembles the splitting of SPR in 1D metallic nanostructures, previously reported in both experiments and simulations.[11] Notably, tubular NP assemblies were rarely observed in previous reports, even for the pure BCP systems.[9]

The tubular and vesicular nature of hollow nanostructures is reflected by the topological features in SEM and the transmission of electron beams in TEM images (Figure 1b−e). In the dehydrated state, the presence of rigid PS and AuNPs inside the shell protected the vesicles and tubules from collapsing. Taking the vesicles as an example, TEM images at multiple tilt angles (−60° to 60°) were recorded using electron microscopic tomography (Figure 1f and SI movie). High-angle images (−60°) clearly presented the vesicle with a well-defined hollow cavity created by a single layer of AuNPs well-packed in the membranes. The observed vesicle is slightly oblate and flattened during drying, as the height (355 nm) was smaller than its diameter (392 nm).

dx.doi.org/10.1021/ja3032295 | J. Am. Chem. Soc. 2012, 134, 11342−11345

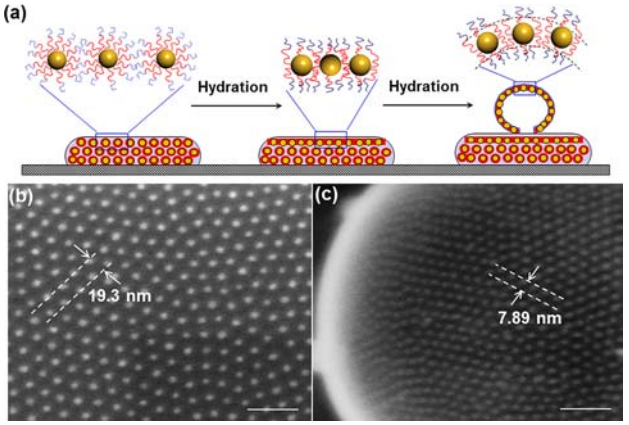

Figure 2. (a) Self-assembly of Au-BCPs by rehydration. (b,c) SEM images of AuNP array before (b) and after (c) vesicular self-assembly, showing the decrease of D_{Au} from 19.3 to 7.89 nm. Scale bars, 100 nm.

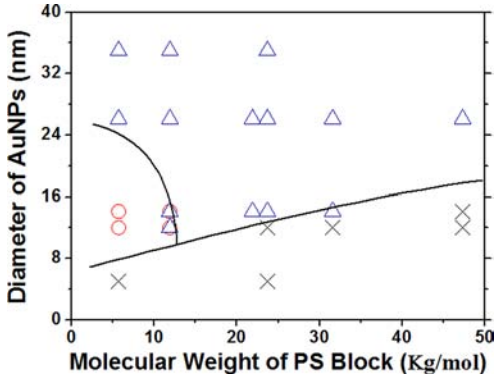

Figure 3. Self-assembly "product diagram" with varying diameter of AuNPs and molecular weight of PS block. The dashes lines indicate the given morphology transition boundary; △, vesicles; ○, tubules; and ×, precipitates.

Aware of the isotropic properties of BCP-tethered colloidal AuNPs in terms of their geometries and chemical functionalities, we proposed a mechanism based on conformation-driven self-assembly of the BCP chain (Figure 2a). In the thin film, the BCP chains are uniformly distributed on the AuNP surface with separated sequences of each block as polymer shells. When the film was sonicated or heated in water, the BCP tethers were partially swollen by water permeated through the defects in AuNP and polymer layers. To minimize interfacial energy, the polymer chain conformation rearranged from isotropic to asymmetric distribution on the surface of AuNPs. In that way, hydrophilic blocks of $PMEO_2MA$ or PEO are fully exposed to water media in the vicinity of the solid/water interface, while PS blocks are shielded from solvents, to achieve favorable enthalpy. With further rehydration, the films detach, roll over, and rearrange by reuniting their edges in order to minimize interfacial energy. Closure of the NP membrane to form a sealed cavity resembles the classic formation of BCP vesicles reported previously.[12]

The mechanism we propose is supported by experimental evidence. First, the interparticle spacing, D_{Au}, of 7.9 nm between adjacent AuNPs of vesicles was only 40% of that in thin films (19.3 nm) (Figures 2b,c and S9). The profound decrease of D_{Au} in the assemblies suggests that the BCP chains are highly stretched toward the polymer/solvent interface to maximize the exposure of hydrophilic blocks to solvents and shield the hydrophobic chains from solvents. Second, AuNPs modified with only $PMEO_2MA$, PEO, or PS using the same procedures could not assemble under the conditions used in BCP systems. AuNPs grafted with only PS cannot be rehydrated from thin films, while AuNPs modified with only $PMEO_2MA$ or PEO are well dispersed in water as individuals. This suggests the self-assembly is driven by the conformational arrangement of BCPs chains, in contrast to previous studies based on phase segregation of multiple grafted polymers or polymers with NP cores.[8a]

Self-assembly of such ACMs predominantly depends on the hydrophilic/hydrophobic balance, i.e., the relative size of hydrophilic/hydrophobic constituents. We systematically investigated the factors that influence the assembled nanostructures by varying the diameter of AuNPs (d_{Au} = 5, 12, 14, 26, 35, 48, 53, and 73 nm) and the length of PS block (R_0 from 5.0 to 14.2 nm) at fixed length of PEO (P2−P7) (Figures S12 and S13). The assembly behavior of ACMs is strongly correlated to the relative size of AuNPs and PS block in BCPs, characterized by the ratio of R_0/d_{Au}. To roughly quantify the results, for $R_0/d_{Au} < 0.5$, Au-BCPs can favorably assemble into vesicles, while for $R_0/d_{Au} \approx 0.5$, tubules are preferred. When $R_0/d_{Au} > 0.5$, Au-BCP cannot be rehydrated in water. This observation is significantly different from previous study on V-shaped polymer tethered NPs, where assembly requires $R_0/d_{Au} > \pi$.[13] This also suggests a new mechanism of BCP-assisted self-assembly of NPs. This assembly of Au-BCPs is summarized in a product diagram in Figure 3. For instance, at fixed M_n of BCPs (i.e., 7.7K), we observed the morphological transition of self-assemblies from insoluble precipitates, tubules, to vesicles by increasing the size of NPs. These results can be explained by the variation in hydrophilicity of ACMs, which is determined by the density of hydrophilic terminals (PEO blocks) on the surface of ACMs (d), as described by the equation, $d = \sigma/[4(0.5 + R_0/d_{Au})^2]$, where σ is the grafting density of BCPs on AuNPs (see SI for details). The density of a hydrophilic block on the surface of ACMs exponentially decreases with increasing R_0/d_{Au} (the length of hydrophilic blocks is neglected to simplify the calculation). The transition density is close to 0.025 chains/nm^2. For $R_0/d_{Au} < 0.5$, higher d value indicates that the higher hydrophilic density is present on the surface of ACMs; thus there is sufficient hydrophilicity to allow the rehydration and assembly of Au-BCPs. However, when $R_0/d_{Au} > 0.5$, the density of hydrophilic chain terminals is less than 0.025, leading to difficulty in rehydrating the BCP-tethered AuNPs.

Other than controlling the assembly morphologies, the molecular weight of BCPs also determines the interparticle spacing D_{Au} between neighboring NPs. Figure 4a−c presents the vesicles prepared from 25 nm AuNPs tethered with P3, P5, and P7 (Figures S16−S20 give more SEM images). Clearly the interparticle spacing displays an obvious increase. The average interparticle spacing, D_{Au}, approximately linearly increased from 5.7 ± 0.9 to 10.9 ± 2.9 nm with the gradual increase in the molecular weight of the PS block from 11.9K to 47.3K g/mol (P3−P7) (Figure 4d), due to the increased volume of PS segments localized between neighboring NPs. We note that the ratio of $D_{Au}/2R_0$ varied in the range of 0.34−0.41, much lower than that of the collapsed polymer chains. This suggests that the PS blocks were partially pulled out of the gaps between the adjacent AuNPs by stretching the BCP chains to maximize the exposure of hydrophilic PEO blocks to surrounding solvent media.[14] The increase of D_{Au} with increasing length of PS

dx.doi.org/10.1021/ja3032295 | J. Am. Chem. Soc. 2012, 134, 11342−11345

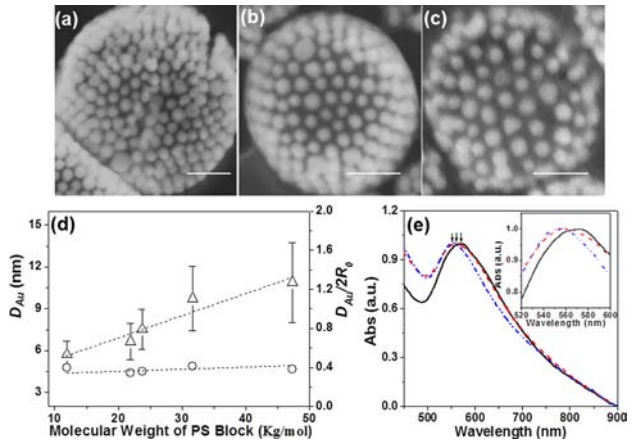

Figure 4. (a–c) SEM images of vesicles assembled from 25 nm Au-P3, Au-P5, and Au-P7. Scale bars, 100 nm. (d) Plot of interparticle spacing D_{Au} (△) and $D_{Au}/2R_0$ (○) as a function of the molecular weight of the PS block. (e) UV–vis spectra of vesicles assembled from 25 nm Au-P3, Au-P5, and Au-P7.

blocks led to a significant blue-shift of the SPR peak from 568 (Au-P3) to 549 nm (Au-P7) (Figure 4e).

In summary, we demonstrate the self-assembly of AuNP amphiphiles designed by grafting amphiphilic BCPs into various hierarchical nanostructures. Re-formation of constituent blocks of BCP chains enables the minimization of interfacial energy, and thus controlled organization of such ACMs into tubular or vesicular assemblies, depending on the AuNPs' size and BCPs' molecular weight. The self-assembled nanostructures may find applications in bioimaging, controlled release, nanophotonics, and nanoelectronics. The exploration of multiphoton excited luminescence of assemblies of AuNPs is ongoing in our laboratory. This phenomenon significantly differentiates our assembly mechanism from those of NPs tethered with a mixture of two homopolymers (or an extreme case of V-shaped BCPs grafted at the junction point of two blocks), where NPs serve as the junctions of hydrophobic and hydrophilic homopolymers. This approach offers precise control over the interparticle distances, thus fine-tuning the plasmonic properties of assembled AuNPs. This strategy can be extended to the assembly of NPs with various shapes (i.e., nanorods and nanoplates) and compositions (see SI). Given current advances in the synthesis of block copolymers with excellent controllability and complexity, our general approach could open up a new realm of possibilities to create libraries of novel colloidal building blocks with predesigned surface chemistry for the fabrication of new functional materials and devices.

■ ASSOCIATED CONTENT

Ⓢ Supporting Information

Details of experiments and characterization. This material is available free of charge via the Internet at http://pubs.acs.org.

■ AUTHOR INFORMATION

Corresponding Author

znie@umd.edu

Notes

The authors declare no competing financial interest.

■ ACKNOWLEDGMENTS

This work is supported by startup funds from the University of Maryland. We thank Prof. Lawrence Sita and Wonseok Hwang for the GPC measurement, Prof. Srinivasa Raghavan for the DLS measurement, and Dr. Li-Chung Lai for the technical assistance on TEM imaging. We acknowledge the support of the Maryland NanoCenter and its NispLab. The NispLab is supported in part by the NSF as a MRSEC Shared Experimental Facilities.

■ REFERENCES

(1) (a) Courty, A.; Mermet, A.; Albouy, P. A.; Duval, E.; Pileni, M. P. *Nat. Mater.* **2005**, *4*, 395. (b) Glotzer, S. C.; Anderson, J. A. *Nat. Mater.* **2010**, *9*, 885. (c) Srivastava, S.; Santos, A.; Critchley, K.; Kim, K. S.; Podsiadlo, P.; Sun, K.; Lee, J.; Xu, C. L.; Lilly, G. D.; Glotzer, S. C.; Kotov, N. A. *Science* **2010**, *327*, 1355. (d) Nie, Z. H.; Petukhova, A.; Kumacheva, E. *Nat. Nanotechnol.* **2010**, *5*, 15. (e) Liu, K.; Zhao, N. N.; Kumacheva, E. *Chem. Soc. Rev.* **2011**, *40*, 656.

(2) (a) Xia, Y. N.; Yin, Y. D.; Lu, Y.; McLellan, J. *Adv. Funct. Mater.* **2003**, *13*, 907. (b) Correa-Duarte, M. A.; Perez-Juste, J.; Sanchez-Iglesias, A.; Giersig, M.; Liz-Marzan, L. M. *Angew. Chem. Int. Ed.* **2005**, *44*, 4375.

(3) (a) Sahoo, Y.; Cheon, M.; Wang, S.; Luo, H.; Furlani, E. P.; Prasad, P. N. *J. Phys. Chem. B* **2004**, *108*, 3380. (b) Leunissen, M. E.; Vutukuri, H. R.; van Blaaderen, A. *Adv. Mater.* **2009**, *21*, 3116. (c) Smoukov, S. K.; Gangwal, S.; Marquez, M.; Velev, O. D. *Soft Matter* **2009**, *5*, 1285.

(4) (a) Mirkin, C. A.; Letsinger, R. L.; Mucic, R. C.; Storhoff, J. J. *Nature* **1996**, *382*, 607. (b) Nykypanchuk, D.; Maye, M. M.; van der Lelie, D.; Gang, O. *Nature* **2008**, *451*, 549. (c) Sharma, J.; Chhabra, R.; Cheng, A.; Brownell, J.; Liu, Y.; Yan, H. *Science* **2009**, *323*, 112.

(5) (a) Zhang, Z. L.; Glotzer, S. C. *Nano Lett.* **2004**, *4*, 1407. (b) DeVries, G. A.; Brunnbauer, M.; Hu, Y.; Jackson, A. M.; Long, B.; Neltner, B. T.; Uzun, O.; Wunsch, B. H.; Stellacci, F. *Science* **2007**, *315*, 358. (c) Wei, Y. H.; Bishop, K. J. M.; Kim, J.; Soh, S.; Grzybowski, B. A. *Angew. Chem. Int. Ed.* **2009**, *48*, 9477.

(6) (a) Zubarev, E. R.; Xu, J.; Sayyad, A.; Gibson, J. D. *J. Am. Chem. Soc.* **2006**, *128*, 15098. (b) Nie, Z. H.; Fava, D.; Kumacheva, E.; Zou, S.; Walker, G. C.; Rubinstein, M. *Nat. Mater.* **2007**, *6*, 609. (c) Wang, B. B.; Li, B.; Zhao, B.; Li, C. Y. *J. Am. Chem. Soc.* **2008**, *130*, 11594. (d) Velev, O. D.; Gupta, S. *Adv. Mater.* **2009**, *21*, 1897. (e) Liu, K.; Nie, Z. H.; Zhao, N. N.; Li, W.; Rubinstein, M.; Kumacheva, E. *Science* **2010**, *329*, 197. (f) Li, F.; Josephson, D. P.; Stein, A. *Angew. Chem., Int. Ed.* **2011**, *50*, 360. (g) He, J.; Yu, B. Y.; Hourwitz, M. J.; Liu, Y. J.; Perez, M. T.; Yang, J.; Nie, Z. H. *Angew. Chem., Int. Ed.* **2012**, *51*, 3628.

(7) (a) Wang, B. B.; Li, B.; Dong, B.; Zhao, B.; Li, C. Y. *Macromolecules* **2010**, *43*, 9234. (b) Song, J. B.; Cheng, L.; Liu, A. P.; Yin, J.; Kuang, M.; Duan, H. W. *J. Am. Chem. Soc.* **2011**, *133*, 10760. (c) Andala, D. M.; Shin, S. H. R.; Lee, H. Y.; Bishop, K. J. M. *ACS Nano* **2012**, *6*, 1044. (d) Wei, K.; Li, J.; Liu, J.; Chen, G.; Jiang, M. *Soft Matter* **2012**, *8*, 3300.

(8) (a) Nikolic, M. S.; Olsson, C.; Salcher, A.; Kornowski, A.; Rank, A.; Schubert, R.; Fromsdorf, A.; Weller, H.; Forster, S. *Angew. Chem., Int. Ed.* **2009**, *48*, 2752. (b) Guo, Y.; Harirchian-Saei, S.; Izumi, C. M. S.; Moffitt, M. G. *ACS Nano* **2011**, *5*, 3309. (c) Li, D. J.; Sheng, X.; Zhao, B. *J. Am. Chem. Soc.* **2005**, *127*, 6248.

(9) Discher, D. E.; Eisenberg, A. *Science* **2002**, *297*, 967.

(10) Rubinstein, M.; Colby, R. H. *Polymer physics*; Oxford University Press: Oxford, U.K., 2003.

(11) Zhong, Z. Y.; Patskovskyy, S.; Bouvrette, P.; Luong, J. H. T.; Gedanken, A. *J. Phys. Chem. B* **2004**, *108*, 4046.

(12) Uneyama, T. *J. Chem. Phys.* **2007**, *126*, 114902.

(13) Zubarev, E. R.; Xu, J.; Sayyad, A.; Gibson, J. D. *J. Am. Chem. Soc.* **2006**, *128*, 4958.

(14) Zhao, B.; Brittain, W. J. *Prog. Polym. Sci.* **2000**, *25*, 677.